Pergamon

Continental Shelf Research, Vol. 15, No. 11/12, pp. 1409–1434, 1995

0278–4343/95 $9.50+0.00

0278–4343(94)00083–2

Tests of bed roughness models using field data from the Middle Atlantic Bight*

J. P. XU†‡ and L. D. WRIGHT†

(*Received* 29 *September* 1993; *in revised form* 22 *March* 1994; *accepted* 15 *June* 1994)

Abstract—Four bottom roughness models are tested using field data from the inner shelf of the Middle Atlantic Bight. Bottom roughness plays a significant role in calculations of sediment concentration profiles and current velocity profiles. The importance of each of the three parts in the roughness models (grain roughness, ripple roughness and sediment motion roughness) vary depending on forcing conditions. Consistent with the observations of others [e.g. Cacchione and Drake, 1990 (*The sea*, Vol. 9, pp. 729–773); Wiberg and Harris, 1994 (*Journal of Geophysical Research*, **99**(C1), 775–7879)], our results show that the models of Smith and McLean (1977; *Journal of Geophysical Research*, **82**, 1735–1746), Grant and Madsen (1982; *Journal of Geophysical Research*, **87**, 469–481) and Nielsen (1983; *Coastal Engineering*, **7**, 233–257) overestimate the sediment transport roughness under sheet-flow conditions. However, the Nielsen (1983) model can predict the ripple roughness under moderate energy conditions quite well. A refined bottom roughness model is proposed that combines Nielsen's ripple roughness model and a modified sediment motion roughness model

$$k_b = d + 8\eta\left(\frac{\eta}{\lambda}\right) + \Omega d(\psi'_m - \psi_c).$$

This sediment motion roughness is defined in such a way that it is proportional to the maximum skin friction Shields' parameter. The proportionality constant, Ω, is determined by fitting the modeled roughnesses and shear velocities with the field observations. The calculated velocity profiles and roughness using the refined roughness model, with $\Omega = 5$, compare well to the field observations made under both moderate and high energy conditions at a sandy inner shelf site.

1. INTRODUCTION

In a wave-dominated continental shelf environment, wave motion interacts with bottom sediment to generate bedforms and sediment transport when wave-induced shear forces exceed a critical value, e.g. the critical Shields' parameter. Both bedforms and sediment transport will increase the total bottom roughness which will then affect the rate of wave energy dissipation. The elements in these processes will adjust themselves until an

*Contribution 1873 from the Virginia Institute of Marine Science.
†Virginia Institute of Marine Science, School of Marine Science, College of William and Mary, Gloucester Point, VA 23062, U.S.A.
‡Present Address: Department of Geography and Anthropology, Louisiana State University, Baton Rouge, LA 70803, U.S.A.

equilibrium is established. A feedback loop linking roughness and friction will operate until the bed shear stress ceases to change and equilibrium is achieved.

Bottom roughness is critical in determining bed shear stress and sediment transport. This problem has been addressed by many investigators (Nielsen, 1979, 1981, 1983; Miller and Komar, 1980a, b; Grant and Madsen, 1982; Smith and McLean, 1977). The convention is to partition the total bed roughness, k_b, into three parts

$$k_b = k_{bd} + k_{br} + k_{bm} \tag{1}$$

where k_{bd} is the grain roughness (usually equal to the grain size, d, multiplied by a constant with a value in the range of $1 \sim 2.5$), k_{br} is form drag roughness (ripple or biological roughness) and k_{bm} is the roughness caused by sediment motion (transport). The last two terms are referred to as movable bed roughness. The significance of each term is relative and related to the sediment properties and flow hydrodynamics. They depend on the amount by which the maximum skin friction Shields' parameter, ψ'_m, exceeds the critical Shields' parameter, ψ_c, for the native sediment. Under very low flow conditions when $\psi'_m < \psi_c$, no ripples are generated on the bottom and there is no sediment transport. Therefore only grain roughness is important when $\psi'_m < \psi_c$ except in situations where residual ripples or biogenic roughnesses are present. If previous ripples and/or biogenic roughness exist, as is commonly the case, both will affect the bed roughness. When flow conditions increase and the skin friction Shields' parameter barely exceeds the critical Shields' parameter of the sediment, pre-existing bedforms and biogenic roughness, if any, will be remolded. Since there is little sediment transport at this stage, form drag roughness makes the most important contribution. During storm conditions (high waves), the bottom shear stress is high and ripples are wiped out; sediment motion roughness (sheet-flow) then dominates (Grant and Madsen, 1982; Wilson, 1989; Nielsen, 1992). Of the three components of bed roughness, the grain roughness, k_{bd}, is the one about which there is the most agreement (Grant and Madsen, 1982; Nielsen, 1981, 1983, 1992; Smith and McLean, 1977). Therefore, k_{bd} will not be critically assessed in this paper. The remaining two parts, k_{br} and k_{bm}, are studied by using the field data to test the performances of several bottom roughness models. Refinements to existing movable roughness models are offered.

2. THE STUDY SITE

The data from two tripod deployments are used here. The deployments were carried out in autumn of both 1991 and 1992 on the inner shelf off the U.S. Army Corps of Engineers Field Research Facility (FRF) at Duck, North Carolina (Fig. 1). The Duck FRF (36°11.1'N, 75°44.4'W) has been the site of many field experiments on the inner shelf (Mason *et al.*, 1987; Green, 1987; Kim, 1991; Wright *et al.*, 1986, 1991, 1992, 1994; Madsen *et al.*, 1993). The tripod in this study was deployed at depths of 13 m in 1991 and 14 m in 1992. Shore-normal bathymetric profiles show that the inner shelf is concave upward over the region and the bathymetry is uniform alongshore (Green, 1987). The bed sediment at this site is composed of about 80% fine to very fine sand and 20% silts and clays. Divers' observations as well as photographs from a profiling camera (Diaz and Schaffner, 1988) indicated the existence of ripples on the bottom at all times during fairweather and moderate seas. (No diver observations have been made during storms.) Ripple lengths were 15–20 cm and ripple heights 2–5 cm. The annual average significant wave height at the

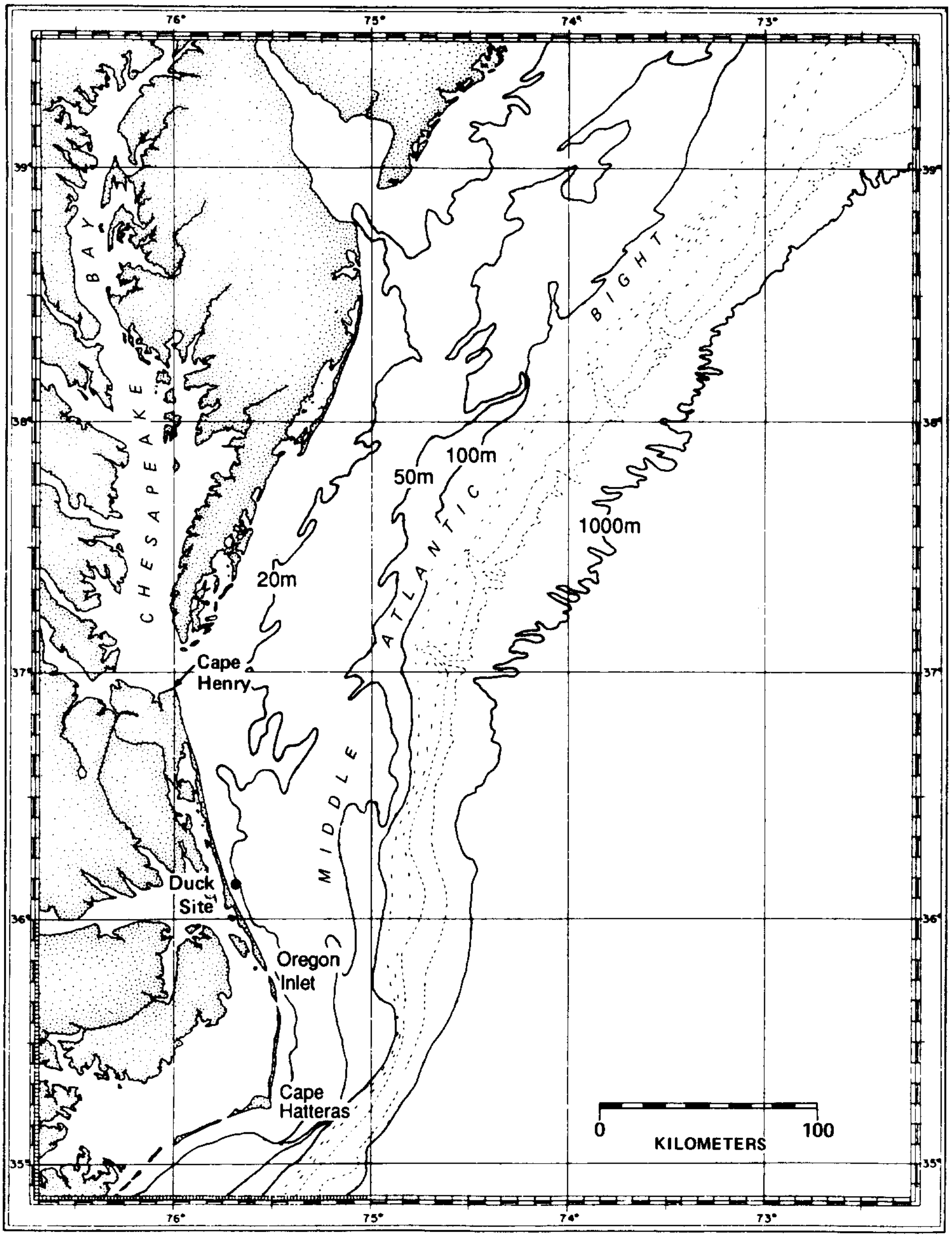

Fig. 1. Location of the experiment site.

end of the FRF Pier is 0.9 m and the annual average peak period is 8.7 s (Birkemeier *et al.*, 1985). Waves are lowest from April to September, and highest from October to December. Extratropical storms ("northeasters") may generate waves with significant heights in excess of 4 m during the period October–February (Birkemeier *et al.*, 1981). Tropical cyclones also generate large waves but are less important over the long term. Waves approach mainly from the south in spring and summer and the north and northeast in the autumn and winter storm season. Extremely high waves and strong wind-driven currents are usually associated with the northeasterly storms. Semi-diurnal tidal range averages 1 m and 1.2 m for spring tides (Birkemeier *et al.*, 1981) and shore-parallel near bottom tidal currents typically have speeds of 10–20 cm s^{-1} (Wright *et al.*, 1991).

3. THE INSTRUMENTATION AND DATA

The instrumentation system used to obtain field data consisted of a tripod frame supporting a Seadata Model 635 directional wave gage incorporating a pressure transducer and a single Marsh–McBirney two-axis electromagnetic current meter, an array of five optical backscatterance sensors, a digital sonar altimeter and an array of three Marsh–McBirney electromagnetic current meters. All of the electromagnetic current meters were 3.8 cm in diameter. One of these systems was deployed at a depth of 13 m in late October 1991. Three of the current meters on the tripod were situated at elevations of 29, 87 and 124 cm; these sensors were logged by means of a Seadata Model 626 electronics package and were sampled at 1 Hz with a burst interval of 4 h and a burst duration of 17 min. The fourth current meter, Model 635, was situated at an elevation of 38 cm and sampled at 5 Hz. All current meters were individually calibrated in steady flows before each deployment using a recirculating flume (Wright *et al.*, 1991). The tripod was deployed from the R.V. *Cape Hatteras* on 16 October 1991. A few days after the deployment, on 20 October, a typical autumn frontal system passed over the coast bringing northeasterly winds that generated a southerly setting current and waves with heights of 1.5 m and periods of 7–8 s. This moderate northeaster provided a valuable typical case for comparison with the more severe storm (the "Halloween" storm) that began on 26 October and eventually subsided on 1 November (Fig. 2). The tripod was broken up on the evening of 30 October. However, the uppermost portion of this tripod including broken sensors and cylinders containing data loggers washed ashore 3 km to the south of the deployment site on 2 November. The data from the Seadata Model 635 system were too badly corrupted to be usable and the digital sonar altimeter and its recorder were missing. The tape containing data from the other three electromagnetic current meters was intact and nearly full of high quality data. In addition, after treatment to remove a corrosive film caused by flooding of the OBS data logging canister, the magnetic disk containing the OBS data was made readable and all of the data were recovered.

A newly constructed tetrapod was deployed at h = 14 m near the 1991 site over the period 28 October–23 November 1992. The tetrapod had an array of four electromagnetic current meters located at 10, 40, 70 and 100 cm above the bottom. Data were logged by ONSET solid state recorders. All instruments were sampled at 1 Hz with a burst interval of 3 h and a burst duration of 34 min. As in 1991 deployment, current meters were individually calibrated in steady flows before each deployment using a recirculating flume (Wright *et al.*, 1991). Moderate energy conditions generally prevailed during the deployments (Fig. 3). After retrieval of the instruments, preliminary analysis showed that the current data from the sensor at 40 cm were not usable due to an offset problem. The current data from this sensor are therefore not used in this study.

Five input parameters are needed to test the roughness models. These are: (1) near bottom wave orbital velocity, u_b; (2) wave period, T; (3) reference mean current velocity, U_c; (4) reference height, z_c (at which U_c is measured); and (5) the angle between wave propagation and mean current direction, θ. All of the parameters, except z_c which was

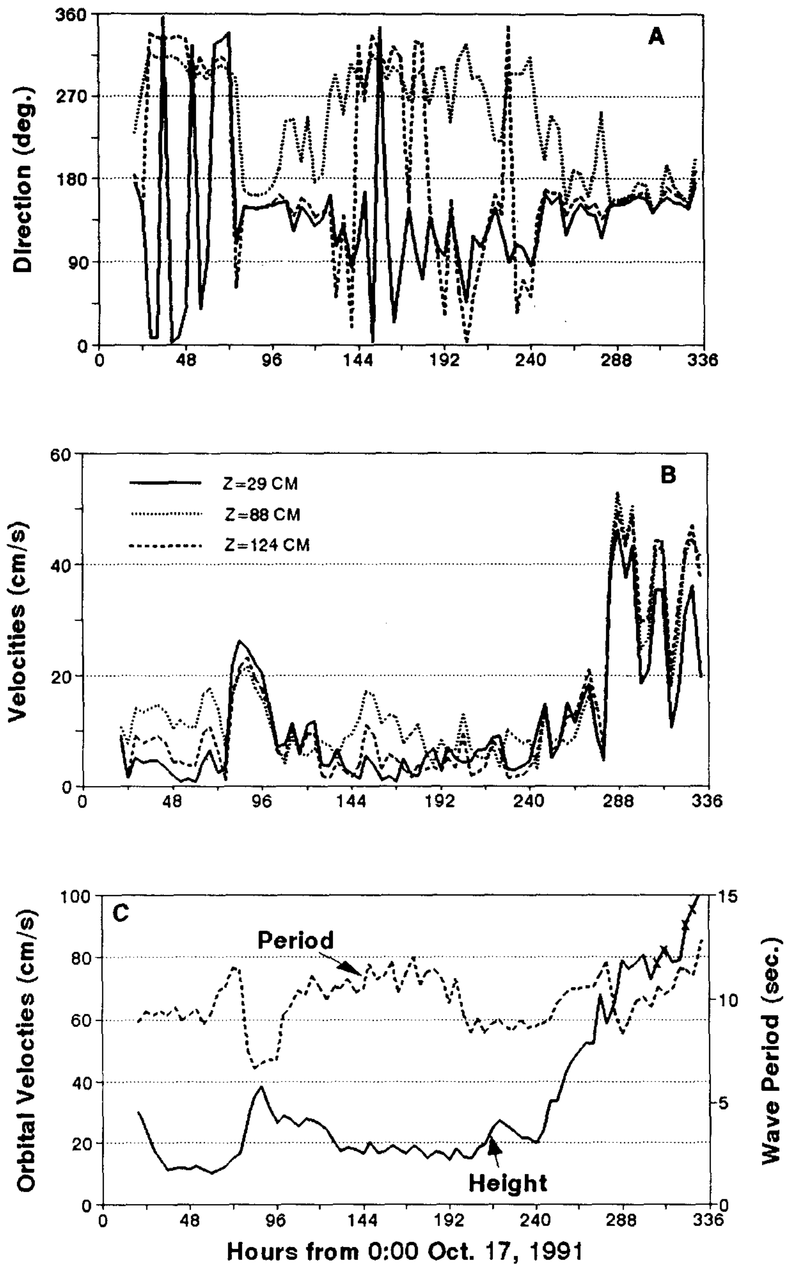

Fig. 2. Measurements from the 1991 deployment. (A) Current direction at three elevations; (B) current speed at three elevations; (C) bottom orbital velocity and wave period. x in the bottom panel denotes the bursts listed in Table 1.

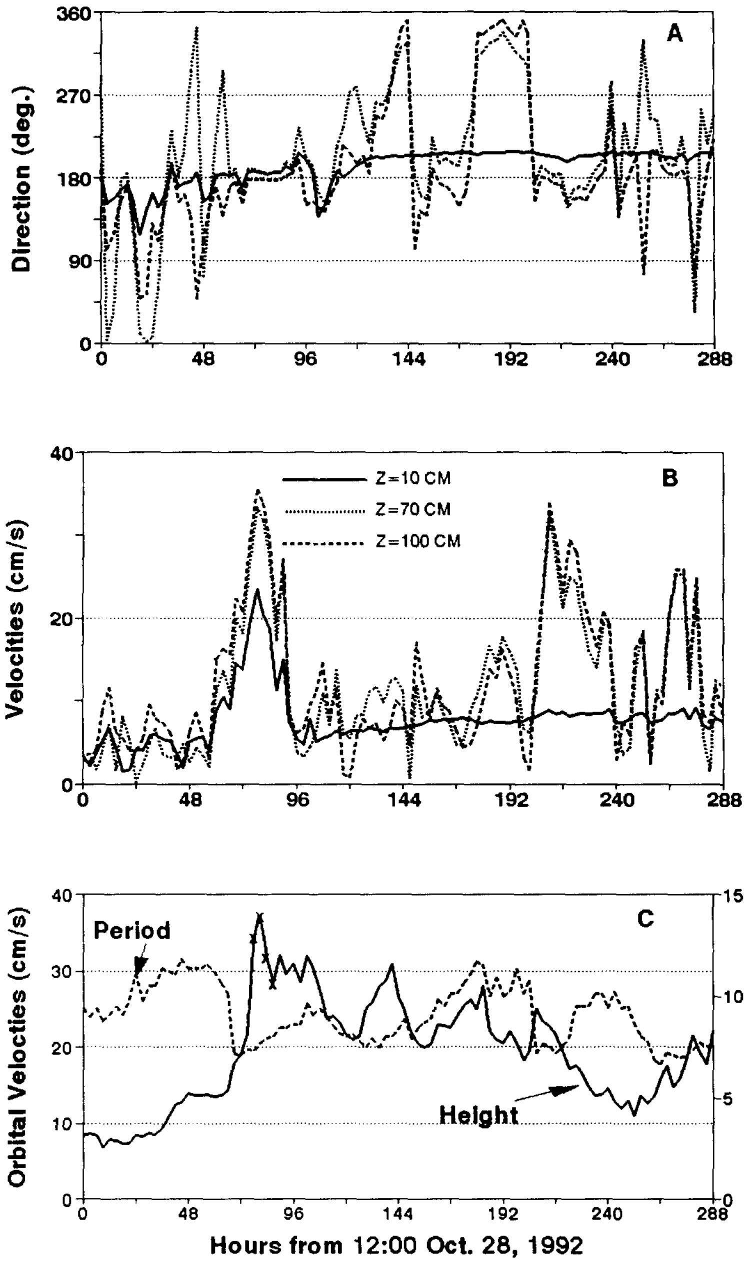

Fig. 3. Measurements from the 1992 deployment. (A) Current direction at three elevations; (B) current speed at three elevations; (C) bottom orbital velocity and wave period. x in the bottom panel denotes the bursts listed in Table 1. The bottom sensor failed after HR96.

Table 1. Input parameters used for the model

Observation	H^*_{rms} (cm)	T (s)	u_b (cm s^{-1})	U_c (cm s^{-1})	z_c (cm)	θ (°)
1992						
HR78	122	7.31	34.5	35.53	100	1.3
HR81	122	7.73	37.3	33.92	100	1.8
HR84	101	7.95	32.0	29.04	100	2.5
HR87	91	8.03	28.5	19.63	100	16.8
1991						
HR308	215	10.6	78.8	44.2	124	72.1
HR312	230	10.2	82.9	44.2	124	82.4
HR324	244	11.4	90.9	42.3	124	87.7
HR328	257	11.2	96.2	47.0	124	85.3

*H_{rms} is computed from u_b using linear wave theory.

equal to 124 cm and 100 cm in the 1991 and 1992 deployments respectively, are derived through procedures described below.

Current time series were analyzed to determine the burst mean current velocity and direction. Readings from the two axes of the current meters were rotated to the east–west (u) and north–south (v) components based on the reading of the compass which was mounted to the tripod. Burst-averages of two rotated components provided the mean current velocity, U_c, and mean current direction, θ_c.

Since the variance of wave orbital velocity attains its maximum in the direction of wave propagation, the wave propagation direction, θ_w, can be determined by rotating the coordinates counterclockwise from the east–west axis until the variance of the rotated components reaches the maximum value. The angle between current and wave directions, θ, was simply the difference of θ_w and θ_c and $\theta < 90°$.

The near-bottom root-mean-square (rms) wave orbital velocity was estimated from

$$u_b = \sqrt{2}\sigma_w \tag{2}$$

where σ_w^2 is the total variance of wave orbital velocity. The wave period, T is evaluated using the zero-crossing of the time series of wave orbital velocity, which is the projection of u and v on the axis of the wave propagation direction.

The eight bursts of hydrodynamic information used in this study are listed in Table 1. The first four bursts are selected from Fig. 3, representing moderate energy conditions. The other four bursts are selected from Fig. 2 to represent the high energy conditions. In selecting the data in Table 1, the following two criteria (Madsen *et al.*, 1993) were applied: (1) to ensure magnitude consistency, the burst-averaged current velocity measured from higher elevations had to be greater than that from below and the vertical velocity profile (3 points) had to be nearly logarithmic; (2) for directional consistency, the directional differences among the burst-averaged current at three elevations must have been less than 8°. As indicated in Fig. 2, there were only four bursts in the 1991 time series which satisfy the two conditions. The other four bursts are taken from the 1992 time series. The eight bursts of measured current velocities and their directions are listed in Table 2. The

Table 2. Measurements of the current profile and estimated current shear velocity and apparent bed roughness

Observation	U_c (cm s^{-1}) 10 cm	70 cm	100 cm	θ_c° 100 cm	$\Delta\theta_c^\circ$	u_{*c} (cm s^{-1})	z_{0a} (cm)	R^2
1992								
*HR*78	23.50	33.39	35.53	94.7	6.7	2.07	0.11	0.999
*HR*81	20.60	31.83	33.92	95.3	6.7	2.31	0.28	0.999
*HR*84	18.67	27.02	29.04	95.6	3.8	1.78	0.15	0.998
*HR*87	11.17	17.28	19.63	103.6	7.5	1.42	0.45	0.984
Observation	U_c (cm s^{-1}) 29 cm	88 cm	124 cm	θ_c° 124 cm	$\Delta\theta_c^\circ$	u_{*c} (cm s^{-1})	z_{0a} (cm)	R^2
1991								
HR308	35.5	42.2	44.2	75.8	4.9	2.40	0.08	0.999
HR312	35.5	43.4	44.2	84.3	1.7	2.56	0.11	0.979
HR324	30.9	41.2	42.3	89.9	7.8	3.34	0.71	0.980
HR328	36.1	44.7	47.0	81.4	7.6	3.03	0.24	0.999

*Degrees counted clockwise from the east (offshore).
u_{*c} Current shear velocity using law of the wall.
z_{0a} Apparent bed roughness using law of the wall.
R_2 Regression coefficient.

hydrodynamic values in Table 1 are input to a boundary layer model (Madsen and Wikramanayake, 1991) to test the bed roughness models discussed in the next section.

4. EXISTING ROUGHNESS MODELS

In order to model the bottom roughness, relations between sediment properties, flow dynamics and ripple geometry must first be obtained. Three important parameters representing the hydrodynamics and sediment properties are involved in these relations. These parameters are: maximum skin friction Shields' parameter, ψ'_m, critical Shields' parameter, ψ_c and the fluid-sediment parameter, S_* (Grant and Madsen, 1982). They are expressed as:

$$\psi'_m = \frac{\tau'_{bm}}{(s-1)\rho g d} \tag{3}$$

$$S_* = \frac{d}{4\nu}\sqrt{(s-1)gd}. \tag{4}$$

If S_* is known, ψ_c can be found directly from the Shields' diagram (Madsen and Grant, 1976). In equation (3), $\tau'_{bm} = 0.5\,\rho f'_w u_{bm}^2$ is the maximum skin friction shear stress, f'_w is the skin friction factor (the method of obtaining f'_w is discussed in the next section) and u_{bm} is the maximum orbital velocity, $\rho = 1020$ kg m^{-3} is sea water density; $g = 9.81$ m s^{-2} is gravitational acceleration, d is sediment diameter taken here as the median diameter, 0.012 cm, $s = \rho_s/\rho$ is the ratio of sediment density, ρ_s, to sea water density, ρ, and ν is the kinematic viscosity of sea water.

Using these parameters, several roughness models have been developed. Based on the data from laboratory-generated bedforms in pure oscillatory flow with several sediment grain sizes, Grant and Madsen (1982) defined two ranges of ripple development. Ripples attain their maximum steepness when $\psi_c < \psi'_m < \psi_b$ where ψ_b is the break-off Shields' parameter,

$$\psi_b = 1.8\, S_*^{0.6} \psi_c. \tag{5}$$

In this range, the following empirical ripple geometry relations were obtained using Carstens' *et al.* (1969) laboratory measurements of wave energy dissipation,

$$\frac{\eta}{A_b} = 0.22 \left(\frac{\psi'_m}{\psi_c}\right)^{-0.16} \tag{6}$$

$$\frac{\eta}{\lambda} = 0.16 \left(\frac{\psi'_m}{\psi_c}\right)^{-0.04} \tag{7}$$

where η is the ripple height, λ is the ripple length and $A_b = u_{bm}/\omega$ is the orbital excursion amplitude. When $\psi'_m > \psi_b$, (break-off range in which the steepness of the ripples decrease), Grant and Madsen (1982) found a different set of ripple geometry relations

$$\frac{\eta}{A_b} = 0.48\, S_*^{0.8} \left(\frac{\psi'_m}{\psi_c}\right)^{-1.5} \tag{8}$$

and

$$\frac{\eta}{\lambda} = 0.28\, S_*^{0.6} \left(\frac{\psi'_m}{\psi_c}\right)^{-1.0}. \tag{9}$$

Using ripple geometries based on the above equations and applying a scaling analysis of the law of the wall and using Wooding's *et al.* (1973) roughness configuration, Grant and Madsen (1982) obtained an empirical ripple roughness relation for a fully rough flow over a rippled bed,

$$k_{b_r} = 27.7 \eta \left(\frac{\eta}{\lambda}\right). \tag{10}$$

There are two simplifying assumptions involved in equation (10). First, the ripples are approximated as two-dimensional roughness elements. Second, the width of the ripple crest in the streamwise direction is of the same order as the height of the ripple.

Nielsen (1981) also derived a set of empirical relations for ripple geometry and ripple roughness based on his analysis of field data (irregular waves) by Inman (1957), Dingler (1975) and Miller and Komar (1980a,b):

$$\frac{\eta}{A_b} = 21 \theta^{-1.85} \tag{11}$$

and

$$\frac{\eta}{\lambda} = 0.342 - 0.34\, \psi'^{0.25}_m. \tag{12}$$

In equation (11), θ was defined as

$$\theta = \frac{u_{bm}^2}{(s - 1)gd}. \tag{13}$$

Using Carstens' *et al.* (1969) and Lofquist's (1986) laboratory measurements of wave energy dissipation, Nielsen (1983, 1992) obtained a relation similar to equation (10) but with a different constant

$$k_{br} = 8\eta\left(\frac{\eta}{\lambda}\right). \tag{14}$$

When ψ'_m exceeds a critical value (e.g. 0.8, Wilson, 1989), the ripples are washed out and the bed becomes flat. However, at this high energy stage, sheet-flow occurs and there is a near-bottom layer of intensive sediment transport (Grant and Madsen, 1982). This sediment transport layer will increase the effective bottom roughness (Nielsen, 1983).

In analogy with Owen's (1964) study of sand grain saltation in air, Smith and McLean (1977) and Grant and Madsen (1982) theoretically derived formulations to estimate the roughness due to sediment motion (transport). Smith and McLean (1977) give

$$k_{bm} = 30\ \alpha_0 d\ (\psi'_m - \psi_c) \tag{15}$$

whereas Grant and Madsen (1982) give

$$k_{bm} = 160\ (s + C_m)d(\sqrt{\psi'_m} - 0.7\ \sqrt{\psi_c})^2 \tag{16}$$

where $\alpha_0 = 26.3$ is an empirical constant and $C_m = 0.5$ is the added mass coefficient for a sphere. Both formulations were derived by using an argument, similar to Owen's, to estimate the thickness of the saltation layer in water. However, Smith and McLean evaluated the coeficient in (15) using unidirectional flow data from the Columbia River while Grant and Madsen set the coefficient in (16) using oscillatory flow data collected by Carstens *et al.* (1969) (Wiberg and Rubin, 1989).

Nielsen (1983) questioned the rationale of equation (16). He argued that the vertical length scale of the sediment motion derived from the idea that a sand grain that hits the bed with horizontal velocity v_i and then bounces off vertically and reaches a height of order of magnitude $v_i^2/2g$, should not be used in water because the relative density of sand to water is a thousand times smaller than the relative density of sand to air. Hence, in water a sand particle will only move a distance comparable to its own diameter before its initial upward velocity vanishes. Using Carstens' *et al.* (1969) laboratory data, Nielsen (1983) obtained, as a best fit, a sediment transport roughness of

$$k_{bm} = 190d(\psi'_m - \psi_c)^{1/2}\ . \tag{17}$$

In a recent study, Madsen *et al.* (1993) estimated the physical bed roughnes under sheet-flow conditions (flat bed) using field data from the October 1991 storm at Duck. The apparent roughness was first obtained using the law of the wall. This apparent roughness, along with other parameters, such as the current shear velocity, were input to a boundary layer model (Grant and Madsen, 1986) to estimate the "real" bottom roughness by removing the wave–current interaction effect (Madsen *et al.*, 1993). The bottom roughness was found to be approximately equal to 15 times the modal grain diameter, d, i.e.

$$k_{bm} = 15d = 0.18\ \text{cm} \tag{18}$$

under the sheet-flow condition which occurs when $\psi'_m > 0.8$ (Wilson, 1989) or $\psi^m > 0.5$ (Katori *et al.*, 1981). Henceforth, $\psi'_m > 0.8$ is used as the criteria of sheet-flow occurrence.

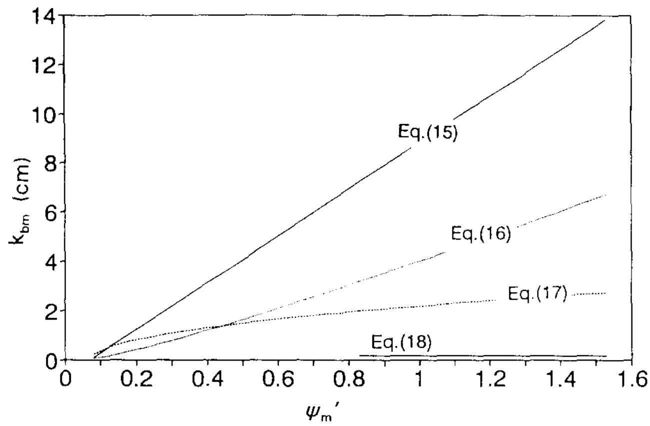

Fig. 4. Comparison of four sediment motion roughness models.

Figure 4 shows the plots of equations (15), (16), (17) and (18) with ψ_c fixed at 0.07. [Although Nielsen (1981) generally assumed $\psi_c = 0.05$, Maa *et al.* (1993) obtained a value of $\psi_c \sim 0.07$ at Duck using a seabed flume.] It is noticed that the model of Smith and McLean (1977) gives the highest estimate of k_{bm} and Madsen *et al.* (1993) gives the lowest.

Combining the expressions of grain roughness, ripple roughness and sediment motion roughness, the four existing roughness models described above can be formulated as follows:

Model 1: Grant and Madsen (1982)

$$k_b = d + 28\eta\left(\frac{\eta}{\lambda}\right) + 430d(\sqrt{\psi_m'} - 0.7\sqrt{\psi_c})^2; \tag{19}$$

Model 2: Nielsen (1983)

$$k_b = 2.5d + 8\eta\left(\frac{\eta}{\lambda}\right) + 190d(\psi_m' - \psi_c)^{1/2}; \tag{20}$$

Model 3: Smith and McLean (1977)

$$k_b = d + 789d(\psi_m' - \psi_c); \tag{21}$$

Model 4: Madsen *et al.* (1993)

$$k_b = d + 15d \qquad \psi_m > 0.8. \tag{22}$$

Models 3 and 4 are used for upper plane flow (sheet flow) conditions only in which no ripple roughness is involved. All four of these roughness models will be tested in the next section.

5. TEST OF ROUGHNESS MODELS USING FIELD DATA

A wave–current combined boundary layer model (Madsen and Wikramanayake, 1991) was used to calculate the current profiles using the four roughness models discussed in Section 4. This boundary layer model is similar to Grant and Madsen's (1986) model, the

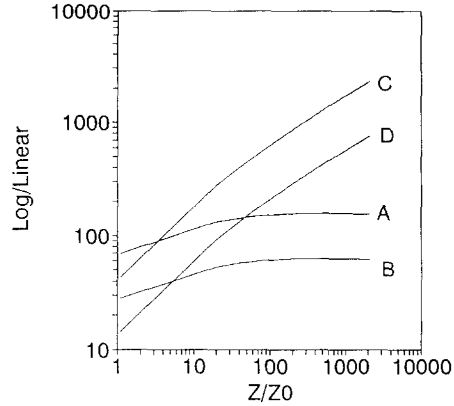

	u_* (cm/s)	z_0 (cm)	γ_0	τ/τ_c
A	3	0.05	4×10^{-4}	10
B	3	0.05	1×10^{-3}	10
C	2	0.05	1×10^{-3}	2
D	2	0.05	3×10^{-3}	2

Fig. 5. Plot of the ratio of the logarithmic to linear term in the corrected law of the wall equation (Gross *et al.*, 1992). The Rouse equation is used to compute the concentration profiles and the Smith and McLean (1977) formula is used to compute the reference concentrations. Other parameters used here are: $\beta = 4.7$; $g = 980$ cm s^{-2}; $w_f = 1.01$ cm s^{-1}; and $c_b = 0.65$.

major difference being that it uses a three-layer continuous eddy viscosity model instead of a two-layer discontinuous eddy viscosity model. The calculated velocity and concentration profiles are smooth in contrast to those from Grant and Madsen (1986) that exhibit kinks. The model employs an approximate friction factor formulation (Grant and Madsen, 1986) in the form of

$$\frac{1}{4\sqrt{f_w}} + \log_{10} \frac{1}{4\sqrt{f_w}} = \log_{10} \frac{A_b}{k_b} - 0.17 + 0.24\,(4\sqrt{f_w}) \qquad (23)$$

to determine the friction factor f_w. To obtain the skin friction factor, f'_w, grain roughness, d, replaces k_b in equation (23). Nielsen used Swart's (1974) formula to compute f'_w; the two f'_w values derived from equation (23) and Swart's formula are almost identical. Grain roughness is defined as equal to the mean grain size by the Grant and Madsen (1982) model and 2.5 times mean grain size by the Nielsen (1983) model in calculation of the skin friction factor. The skin friction factor is then used to calculate the maximum skin friction shear stress, $\tau'_{bm} = 0.5\ \rho f'_w u^2_{bm}$ and physical bottom roughness k_b using the four roughness models. Iterating k_b in equation (23) yields the total friction factor f_w which is then used to calculate the maximum wave shear velocity, the combined shear velocity and the current shear velocity. Using the solutions of Madsen and Wikramanayake (1991), the current profiles were obtained.

The effect of suspended-sediment stratification was not included in the calculations because an examination of this effect following Gross *et al.* (1992) suggested that it was not significant. Figure 5 displays the ratio of the logarithmic term [$\ln(z/z_0)$] to the linear term

Table 3. Output parameters from the model

Observation	Model	η (cm)	λ (cm)	ψ'_m	k_{br} (cm)	k_{bm} (cm)	f_{cw}	u_*^c (cm s^{-1})	u_{*c} (cm s^{-1})	δ_w^* (cm)	z_0 (cm)
1992											
HR87	GM	5.35	42.15	0.15	19.02	0.24	0.14	7.83	2.39	8.01	0.64
	N	0.73	6.11	0.19	0.69	0.76	0.04	4.07	1.57	4.16	0.05
1991											
HR308	GM	0	0	0.86	0	3.25	0.03	9.82	4.07	13.26	0.11
	N	0	0	1.06	0	2.21	0.03	9.10	3.85	12.29	0.07
	SM	0	0	0.86	0	7.26	0.04	11.72	4.64	15.81	0.24
	M	0	0	0.86	0	0.18	0.01	6.00	2.83	8.09	0.01

$^*\delta_w$ is the wave boundary layer depth.
GM Grant and Madsen (1982).
N Nielsen (1983).
SM Smith and McLean (1977).
M Madsen *et al.* (1993).

(correction for stratification) of a log–linear law-of-the-wall equation (Gross *et al.*, 1992). The linear term is computed in its simplest form, $\beta(z - z_0)/L$, where $\beta = 4.7$ is an empirical constant, z is elevation above bottom, z_0 is the hydraulic roughness length scale, and L is the Monin–Obukhov length scale. The four lines in Fig. 5 are computed using the four sets of typical values of shear stress, resuspension coefficient and others which represent the high and moderate energy conditions elucidated in this paper. All four cases in Fig. 5 show that the logarithmic term is at least one order greater than the linear correction term, especially for the elevations where our measurements were made. Therefore, we assume the linear term is not significant and suspended-sediment stratification is ignored.

The boundary layer model was run against the field data of moderate and high (storms) energy conditions listed in Table 1. The output of two example bursts from each of four roughness models are shown in Table 3. It is seen that substantial differences exist among the results from the four roughness models. For moderate energy conditions in which ripple roughness is dominant, the Grant and Madsen roughness model produces quite a large estimate of ripple roughness compared to the Nielsen model. The former (19.02 cm) is almost 30 times higher than the latter (0.69 cm). The typically observed k_b (= 30 z'_o) under these conditions is 3–10 cm (Wright, 1993). Although the sediment motion roughness from the Nielsen model (0.76 cm) is about three times that from the Grant and Madsen model, the total roughness of the Grant and Madsen model is still 13 times that of the Nielsen model. For high energy conditions when the ripple roughness diminishes with increasing bed shear stress and sediment motion roughness dominates, the roughness produced by models 1, 2 and 3 are at least one order of magnitude larger than that obtained by model 4.

Figures 6 and 7 show the calculated current velocity profiles with the above roughness models for moderate and high energy conditions, respectively. Under moderate energy conditions (Fig. 6), when the ripple roughness dominates, the modeled current velocities from the Nielsen (1983) model are much greater than those from the Grant and Madsen (1982) model for $z < 1$ m. This is attributable to the larger roughness (and correspondingly larger shear velocities) generated by the Grant and Madsen (1982) model. Under high

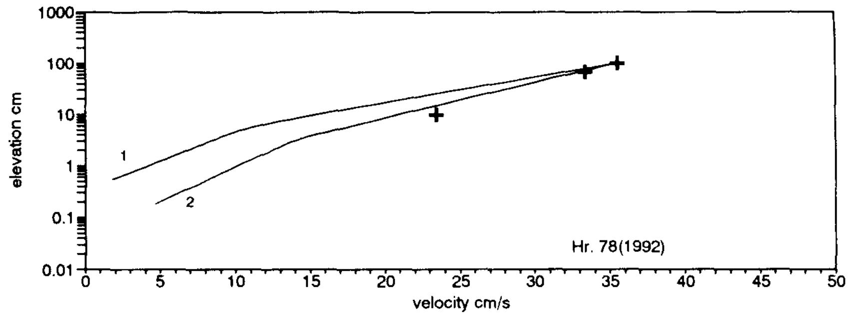

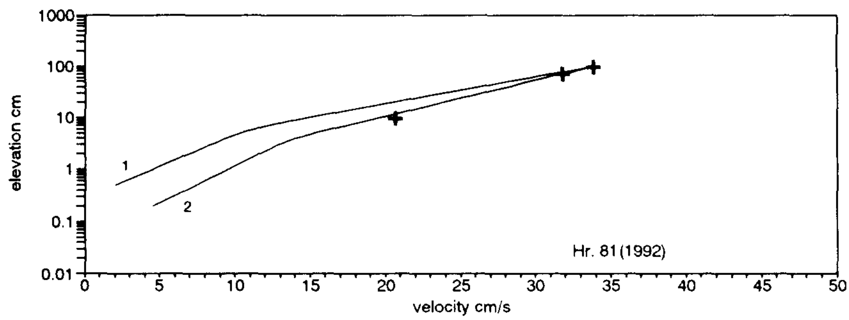

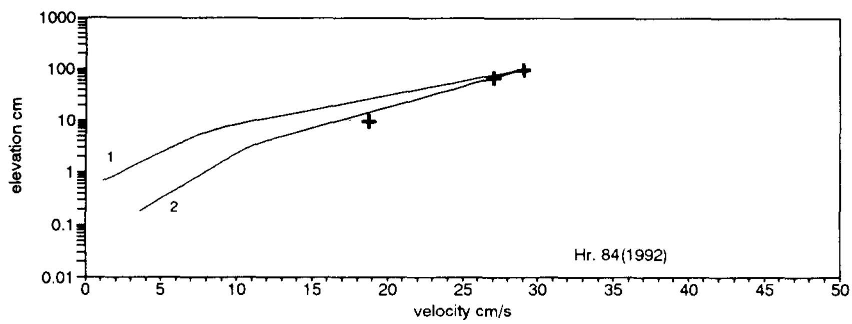

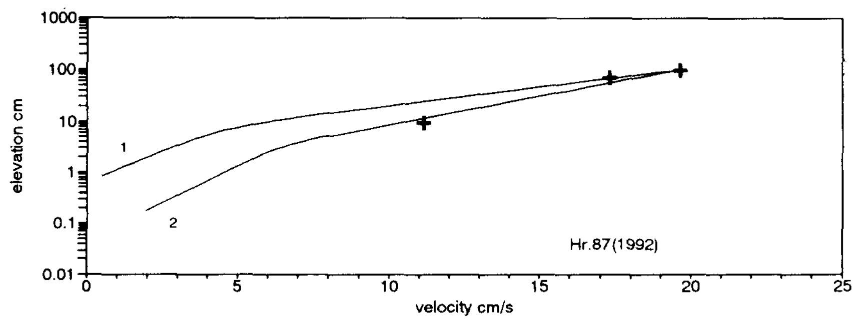

Fig. 6. Comparison of measured and calculated current velocity profiles for the four bursts of moderate energy condition. The numbers (1 and 2) in each panel represents calculated profiles using Grant and Madsen (1982) and Nielsen (1981) roughness models respectively. + denotes the measured profile.

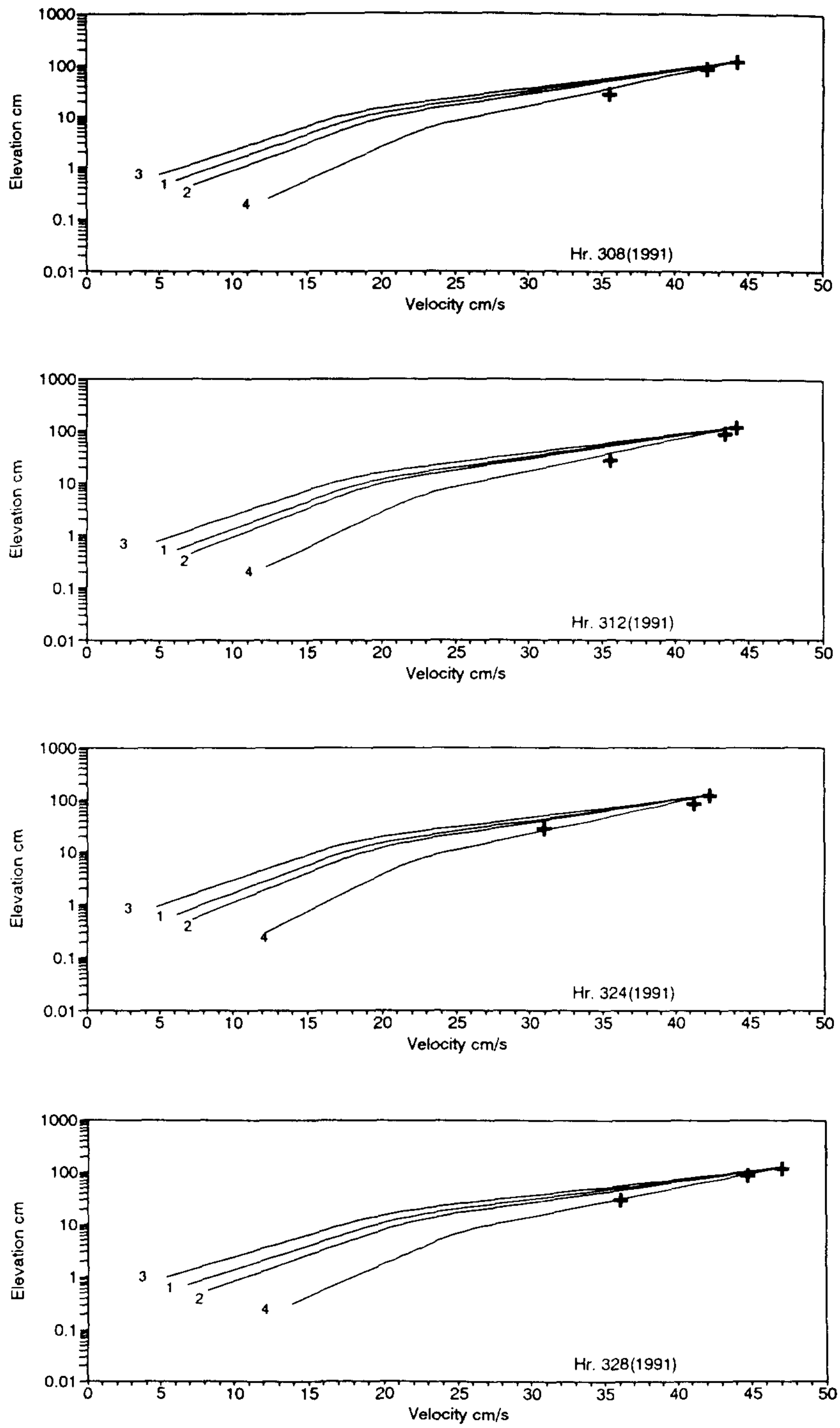

Fig. 7. Comparison of measured and calculated current velocity profiles for the four bursts of high energy condition. 3 and 4 denote the calculated profiles using the Smith and McLean (1977) and Madsen *et al.* (1993) roughness models, respectively. Other notations are the same as in Fig. 6.

energy conditions, the ripples are washed out and ripple roughness is predicted to vanish by all models and the bottom roughness is solely due to sediment transport. Under this circumstance, all four roughness models are employed to compute the velocity profiles (Fig. 7) and to estimate the bottom roughness. The velocity profiles vary depending on the estimated roughnesses and shear velocities which are quite different from one model to another (Table 3). The Smith and McLean model produces the highest shear velocities and the Madsen *et al.* (1993) model gives the lowest.

By comparing the calculated current velocity profiles from both energy conditions with the measured current velocity profiles (denoted by + in each figure), we find that the Nielsen roughness model produces better current velocity estimates than the Grant and Madsen model under moderate energy conditions. Under high energy conditions, the Madsen *et al.* roughness model offers the best estimates of current velocities. This indicates that, at least for our limited data, the Nielsen (1983) roughness model yields better estimates of bed roughness under moderate energy conditions and the Madsen *et al.* (1993) model gives better estimates under high energy conditions.

6. A REFINED ROUGHNESS FORMULATION

The observations just described suggest that a combination of the Nielsen ripple roughness model and the Madsen *et al.* (1993) sediment motion roughness model can produce a better agreement between the calculated and measured velocity profiles at all energy levels. Therefore, a new "composite" roughness formulation is established following this concept.

When the maximum skin friction Shields' parameter exceeds the critical value, ψ'_c, sediment motion is initiated. As ψ'_m increases, more sediment grains start moving and ripples are generated. When ψ'_m continues to increase, sheet flow ultimately occurs because ψ'_m becomes so large that all ripples are wiped out and the bed enters the upper plane condition. Investigators have studied the criteria of sheet flow occurrence and have given different results. Katori *et al.* (1981) found, in their oscillatory flow tank experiments, that sheet flow occurred when ψ'_m exceeded 0.5. Wilson (1988, 1989) studied the sheet flow in a pressurized tube for steady flow and found that the ψ'_m criteria is 0.8. For values of ψ'_m greater than 0.8, the bed is found to be essentially flat, with bed-load particles moving briskly in a sheet flow layer which has thickness, δ_s, much larger than the grain size (Wilson, 1989). δ_s is a function of sediment grain size and ψ'_m. Wilson (1988) reanalyzed his data obtained from two experiments conducted in a pressurized conduit (Wilson, 1966) and showed that

$$\delta_s = 10d\psi'_m. \tag{24}$$

By analogy with the Nikuradse sand grain roughness, Wilson (1988) suggested that roughness under sheet flow conditions is equal to a multiple of δ_s. This multiple is approximately 0.5 (Wilson, 1988), leading to the following expression of the roughness

$$k_{bm} = 5d\psi'_m. \tag{25}$$

Equation (25) was developed for sheet flow conditions in which ψ'_m ($\geq$0.8) is at least an order of magnitude greater than the largest ψ_c of non-cohesive sediments. Due to the small difference between ψ'_m and ($\psi'_m - \psi_c$) it is reasonable to assume that k_{bm} is independent of the sediment grain size. This assumption, however, will no longer be valid when we extend the applicability of equation (25) to flow conditions where ψ'_m is only slightly greater than ψ_c. Equation (25) must be modified to account for the dependence of roughness on sediment grain size. This leads to the following expression

$$k_{bm} = \Omega d(\psi'_m - \psi_c) \qquad \text{for } \psi'_m > \psi_c. \tag{26}$$

This formulation is used in all flow conditions. As long as ψ'_m is greater than ψ_c and sediment grains are in motion, k_{bm} will increase with ψ'_m. In equation (26), Ω is a proportionality constant. When $\Omega = 789$, equation (26) becomes identical to the Smith and McLean model shown in equation (15).

Combining grain roughness, the Nielsen ripple roughness and equation (26), the resulting roughness formulation (Model 5) applicable when $\psi'_m > \psi_c$ is derived

$$k_b = d + 8\eta\left(\frac{\eta}{\lambda}\right) + \Omega d(\psi'_m - \psi_c). \tag{27}$$

In equation (27), η and λ are estimated using the Nielsen (1983) formulations, equation (11) and (12), when $\psi'_m \leq 0.8$. After $\psi'_m > 0.8$, the bottom is flat and the ripple roughness disappears. When $\psi'_m \leq \psi_c$, and there are no pre-existing ripples, equation (27) gives $k_b = d$. The proportional constant, Ω, will be determined through testing procedures using the field data.

Employing equation (27), the boundary layer model is run again using the same data. For each of the eight bursts, the model was run seven times with $\Omega = 1, 5, 10, 15, 30, 50$ and 100, respectively. The computed current velocity profiles are plotted in Fig. 8 (moderate energy conditions) and Fig. 9 (high energy conditions). In Fig. 8, the selection of Ω values does not make much difference in the velocity profiles because the bed roughnesses under moderate energy conditions are dominated by the ripples. All seven profiles are more or less the same as that computed using the Nielsen roughness model shown in Fig. 6. The values of Ω are crucial, however, in computing the velocity profiles under the high energy conditions shown in Fig. 9. The flows reach the upper plane stage and all ripples are washed out. It is not clear in Fig. 9 which Ω value produces the best overall approximation to the measured velocity profiles. The figure does show, however, that Ω values in the range of 1–30 are appropriate for our data.

In order for equation (27) and the corresponding figures to make quantitative sense, the calculated and observed bed roughnesses are compared. The observed bed roughness was estimated by the same approach used by Madsen *et al.* (1993). First, the apparent roughness (z_{0a}) and the current shear velocity (u_{*c}) were obtained by applying the law of the wall (Table 2). Then they were input to the Madsen and Wikramanayake (1991) boundary layer model. The boundary layer model was run iteratively until a value of the bed roughness was obtained that reproduces the observed value (from the law-of-the-wall) of the current shear velocity. The effect of the wave–current interaction was removed and the real bed roughness values were obtained. Figures 10 and 11 display the field-observed bed roughnesses (determined from velocity profiles) with the 95% confidence intervals (Gross and Nowell, 1983) together with the values of k_b calculated using the five roughness models for the moderate and high energy conditions, respectively. Equation (27) was applied seven times with various Ω values that are denoted on the horizontal axis. Compared to the field observations, the refined formulation produces the best estimates, with 95% confidence, of bed roughnesses. Because the Nielsen model over-estimates

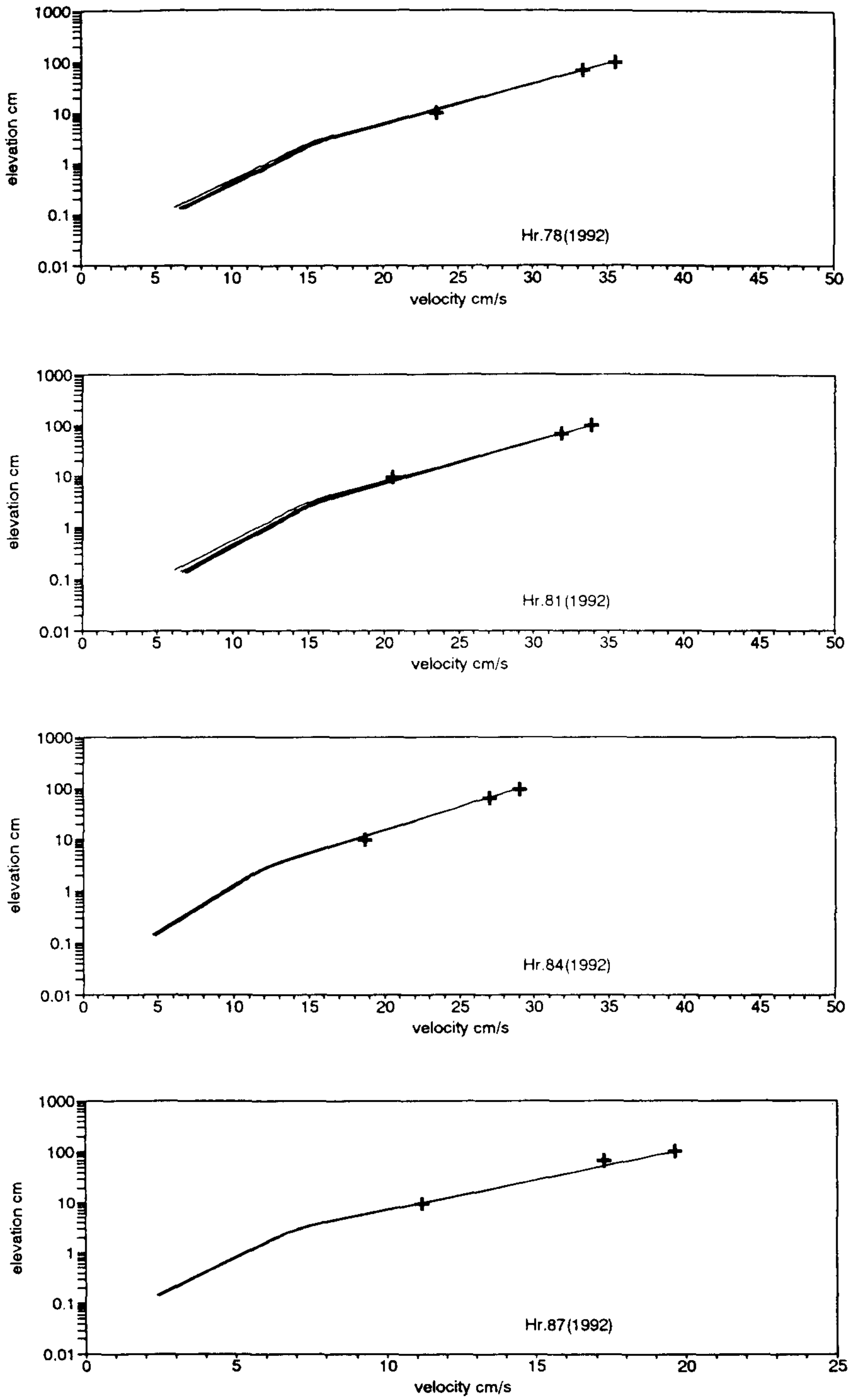

Fig. 8. Comparison of measured and calculated current velocity profiles [using equation (27) with $\Omega = 1, 5, 10, 15, 30, 50$ and 100, respectively] for the four bursts of moderate energy condition. + denotes the measured profile.

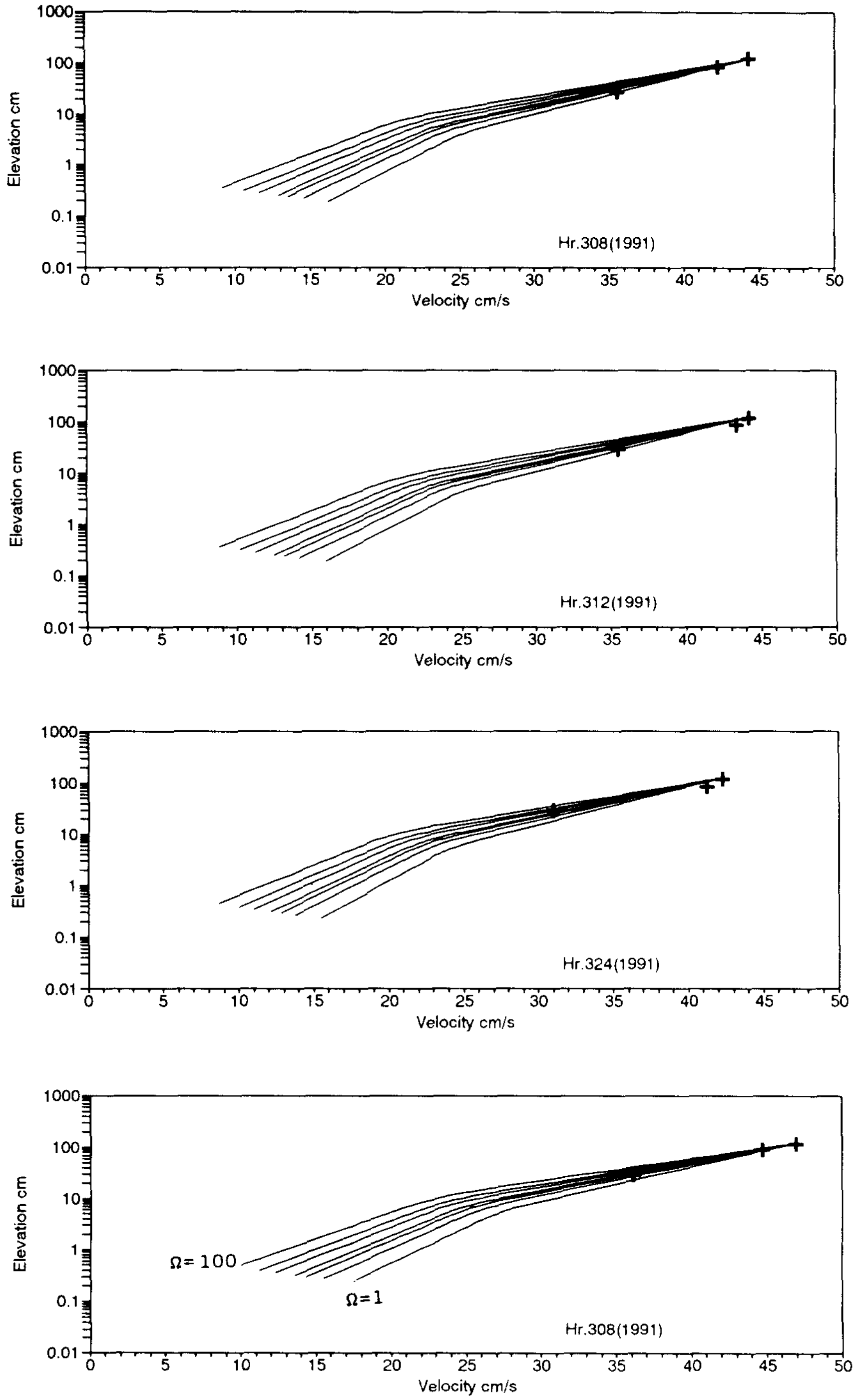

Fig. 9. Comparison of measured and calculated current velocity profiles [using equation (27) with $\Omega = 1, 5, 10, 15, 30, 50$ and 100, respectively] for the four bursts from high energy conditions. The current velocities are the greatest when $\Omega = 1$ and smallest when $\Omega = 100$. + denotes the measured profile.

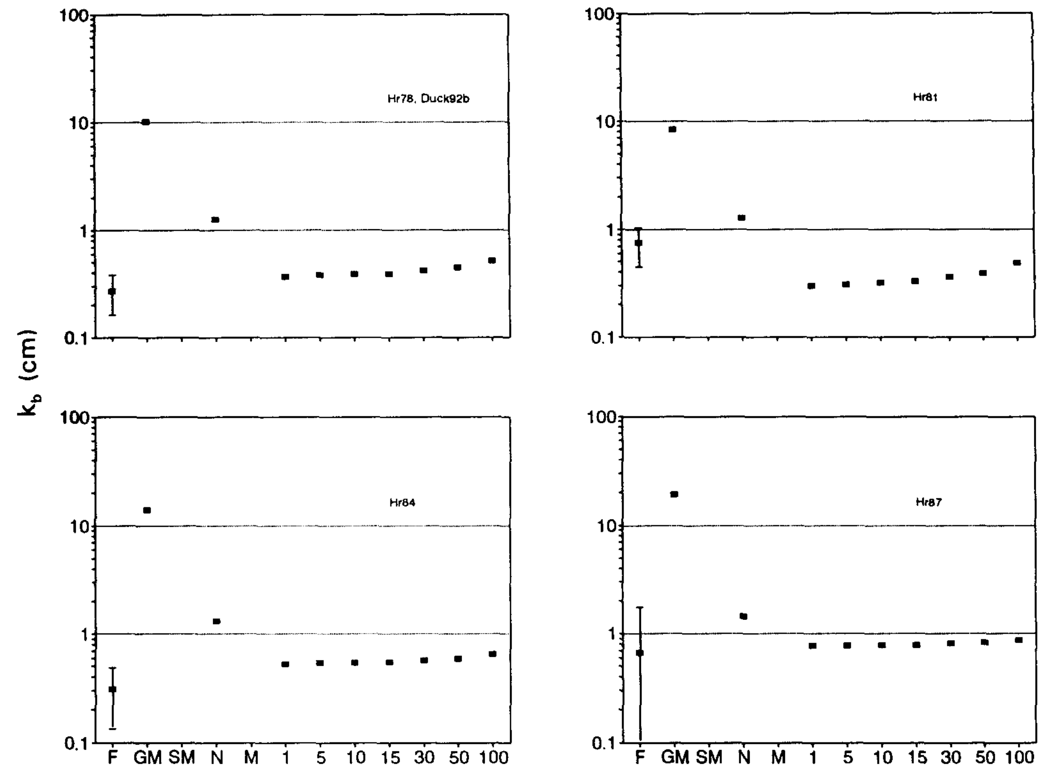

Fig. 10. Comparison of the field-observed and calculated total roughness, k_b, for the four bursts of the moderate energy conditions. F = Field observation, GM = Grant and Madsen, SM = Smith and McLean, N = Nielsen, M = Madsen *et al.* The numbers in the horizontal axis are Ω values when equation (27) is used. The bar indicates the 95% confidence interval.

sediment motion roughness, the associated predicted k_b is much higher than that from the refined formulation; however both models have the same term for ripple roughness.

The relative deviation, E, of the modeled k_b from the field-observed values are calculated using

$$E = \frac{|X_m - X_f|}{X_f}. \tag{28}$$

In the above equation, the subscript m represents a modeled value and f the field-observed value. Figure 12 displays the relative deviation. It shows that the refined formulation with $\Omega = 5$ gives the smallest average deviation, $E \leqslant 0.5$ which is consistent with equation (25).

Applying equation (27) and letting $\Omega = 5$, the bed roughnesses are calculated for the full time series shown in Figs 2 and 3. The results from the moderate energy, 1992 deployment are plotted in Fig. 13 and the high energy, 1991 deployment in Fig. 14. It is shown in both figures that ripple roughnesses dominate ($k_{br} > k_{bm}$) when $\psi'_m > \psi_c$ but $\psi'_m < 0.8$. It is also seen that the ripple roughnesses decrease when ψ'_m is greater than a certain value. This ψ'_m value (0.12) is very close to the break-off Shields' parameter defined by Grant and Madsen (1982) and computed from equation (5). This indicates that the Grant and Madsen concept

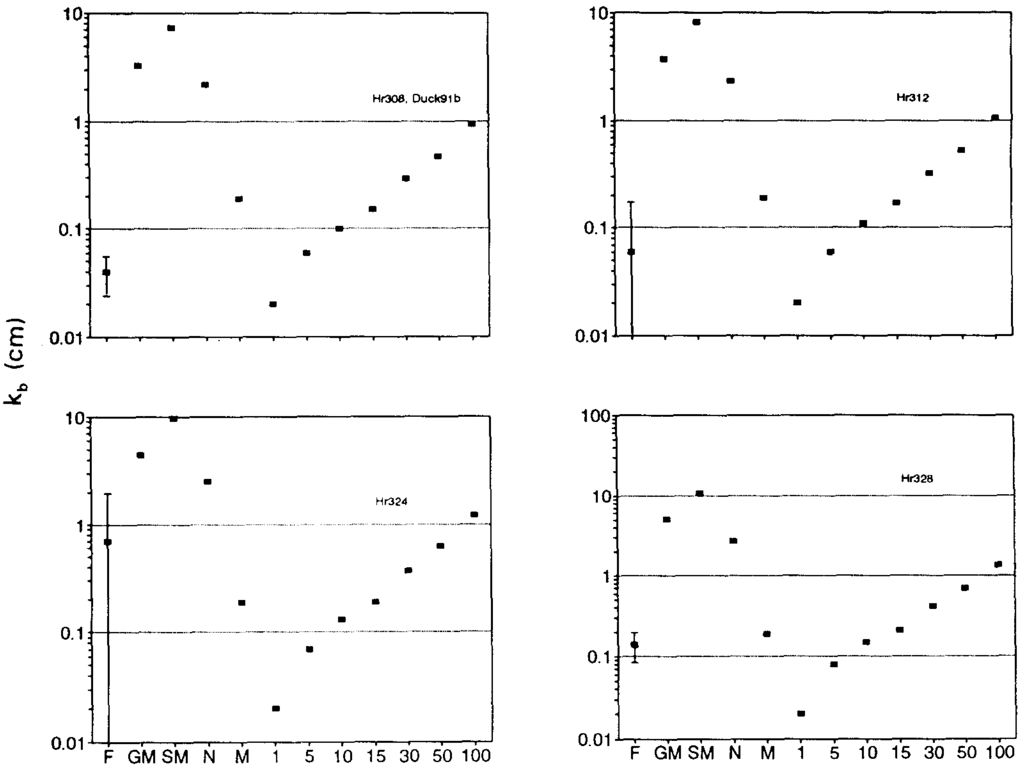

Fig. 11. Comparison of the field-observed and calculated total roughness, k_b, for the four bursts of the high energy conditions. F = Field observation, GM = Grant and Madsen, SM = Smith and McLean, N = Nielsen, M = Madsen *et al.* The numbers in the horizontal axis are Ω values when equation (27) is used. The bar indicates the 95% confidence interval.

of the break-off Shields' parameter works well in the Nielsen ripple roughness model although the latter model does not depict the break-off Shields' parameter explicitly. When the flows reach upper plane conditions and $\psi'_m > 0.8$ (from HR288 to HR336 in Fig. 14), the ripple roughnesses diminish and the sediment transport roughnesses dominate. But the overall roughness (with wave–current effects removed) is at least one order smaller than that when ripples exist. The modeled bed roughnesses compare fairly well to the available roughnesses determined from velocity profiles except for one point in Fig. 14.

7. SUMMARY AND CONCLUSIONS

The roughness values used in boundary layer models are important in determining bottom shear stress, sediment suspension and wave energy dissipation. Our field results indicate that the Smith and McLean (1977), Grant and Madsen (1982) and Nielsen (1983) roughness models all over-estimate the sediment motion roughness under high energy conditions (storm) even though the Nielsen (1983) model can predict the ripple roughness under moderate energy conditions quite well. Similar conclusions have been reached by Cacchione and Drake (1990) and Wiberg and Harris (1994). It is also found that the Madsen *et al.* (1993) roughness model, used only under high energy conditions, gives the

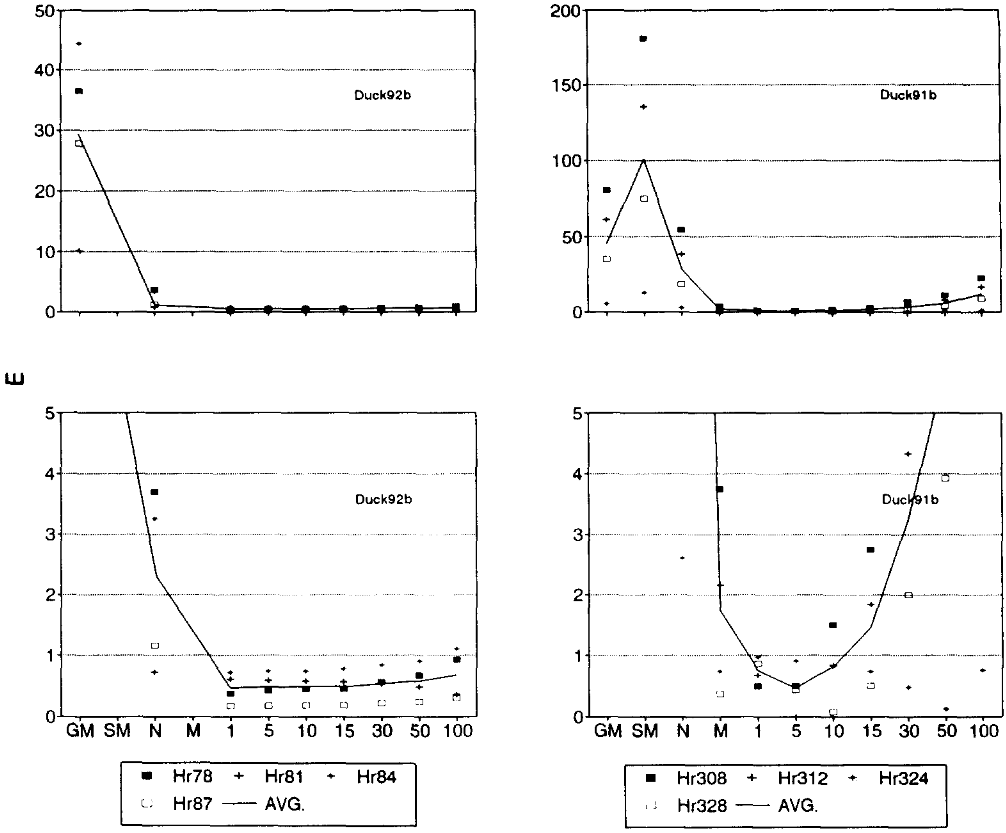

Fig. 12. Plot of the relative deviation, E, of the calculated k_b from the field observations. The two bottom panels show the detail of the lower portion of the two top panels. The symbols denote the four data bursts and the solid line denote the average.

best prediction of current velocity profiles compared to the measurements. Based on comparisons between the measured and calculated velocity profiles, a refined roughness formulation is established [equation (27)]. This model combines the Nielsen (1983) ripple roughness model with a modified sediment motion roughness model. Like previous models, the new roughness model is partitioned into three components: grain roughness, ripple roughness and sediment motion roughness. The sediment motion roughness is defined in such a way that it is proportional to the maximum skin friction Shields' parameter. The calculated velocity profiles using the new roughness model compared well to the measured velocity profiles under both moderate and high energy conditions on the inner shelf when the proportionality constant in equation (27) is equal to 5. The calculated roughnesses using the refined model also compare fairly well to the field observations made under both moderate and high energy (storm) conditions.

The general utility of the refined formulation, especially the proportionality constant Ω, cannot be fully determined until the roughness model is rigorously tested against more field and/or laboratory data. This is particularly the case when recognizing that there are only three points in the measured velocity profiles and there may be measurement errors in these profiles from which the field-observed k_b and u_{*c} are calculated. The assumptions

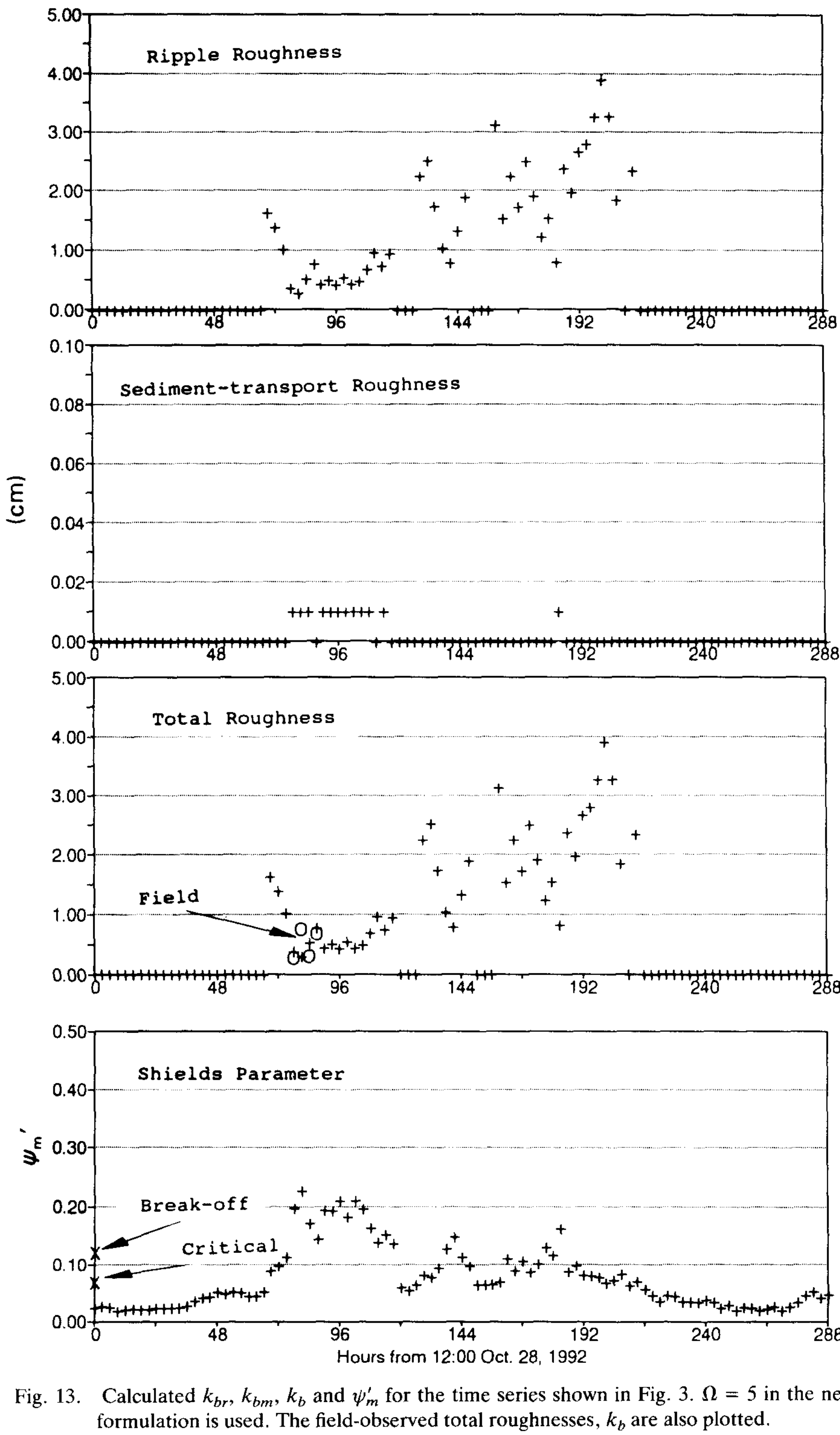

Fig. 13. Calculated k_{br}, k_{bm}, k_b and ψ_m' for the time series shown in Fig. 3. $\Omega = 5$ in the new formulation is used. The field-observed total roughnesses, k_b are also plotted.

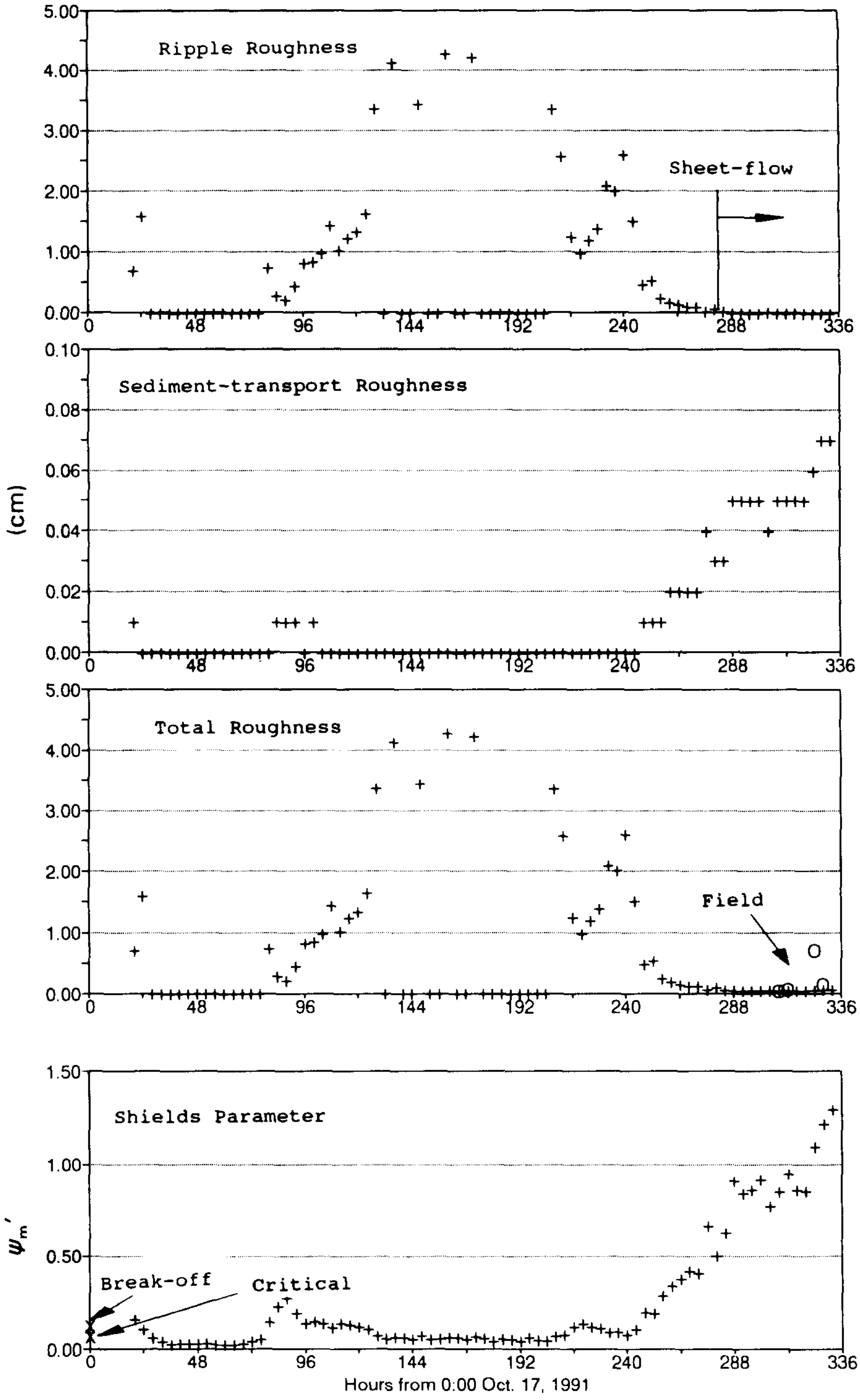

Fig. 14. Calculated k_{br}, k_{bm}, k_b and ψ'_m for the time series shown in Fig. 2. $\Omega = 5$ in the new formulation is used. The field-observed total roughness, k_b are also plotted.

such as linear eddy viscosity profile, zero suspended sediment stratification, and zero armoring effects may not always be valid.

Acknowledgements—This study has been supported by the National Science Foundation, Marine Geology and Geophysics Grant OCE-9017828. We thank J. D. Boon, R. A. Gammisch, D. A. Hepworth and F. H. Farmer for their assistance in the field and with data analyses. Also acknowledged are helpful comments received from two anonymous reviewers. This is contribution number 1873 from the Virginia Institute of Marine Science.

REFERENCES

Birkemeier W. A., A. W. Dewall, C. S. Corbics and H. C. Miller (1981) *A user's guide to C.E.R.C.'s Field Research Facility*, U.S. Army Corps of Engineers, CERC, MR 81-7.

Berkemeier W. A., H. C. Miller, S. D. Eilhelm, A. W. Dewall and C. S. Corbics (1985) *A user's guide to the Coastal Engineering Research Center's* (CERC's) *Field Research Facility*, Instruction Report CERC-85-1, U.S. Army Corps of Engineers, Waterways Experiment Station, Vicksburg, MS, 121 pp.

Cacchione D. A. and D. E. Drake (1990) Shelf sediment transport: An overview with applications to the northern California continental shelf. In: *The sea*, Vol. 9, D. Hanes and B. LeMehaute, editors, pp. 729–773.

Carstens M. R., F. M. Neilson and H. D. Altinbilek (1969) *Bed forms generated in the laboratory under an oscillatory flow: analytical and experimental study*, TM-28, U.S. Army Corps of Engineers, Coastal Engineering Research Center.

Diaz R. J. and L. C. Schaffner (1988) Comparison of sediment landscapes in Chesapeake Bay as seen by surface and profile imaging. In: *Understanding the estuary, advances in Chesapeake Bay research*, M. P. Lynch and E. C. Krome, editors, Chesapeake Bay Research Consortium, CBP/TRS, 24/88, pp. 222–240.

Dingler J. R. (1975) Wave formed ripples in nearshore sands, Ph.D. Thesis, University of California, San Diego, 136 pp.

Grant W. D. and O. S. Madsen (1982) Movable bed roughness in unsteady oscillatory flow. *Journal of Geophysical Research*, **87**, 469–481.

Grant W. D. and O. S. Madsen (1986) The continental shelf bottom boundary layer. *Annual Review of Fluid Mechanics*, **18**, 265–305.

Green M. O. (1987) Low energy bedload transport, Southern Mid-Atlantic Bight, Ph.D. Thesis, School of Marine Science, College of William and Mary, Gloucester Point, VA, 162 pp.

Gross T. F., A. E. Isley and C. R. Sherwood (1992) Estimation of stress and bed roughness during storms on the Northern California Shelf. *Continental Shelf Research*, **12**, 389–413.

Gross T. F. and A. R. Nowell (1983) Mean flow and turbulence scaling in a tidal boundary layer. *Continental Shelf Research*, **2**, 109–126.

Inman D. L. (1957) *Wave generated ripples in nearshore sands*, TM-100, U.S. Army Corps of Engineers, Beach Erosion Board.

Katori S., A. Watanabe and K. Horikawa (1981) Laboratory study on sediment movement in the sheet flow regime. *Coastal Engineering of Japan*, **24**, 235.

Kim S. C. (1991) Inner continental shelf benthic boundary layer dynamics and suspended sediment transport, Ph.D. Thesis, School of Marine Science, College of William and Mary, Gloucester Point, VA, 158 pp.

Maa J. P.-Y., L. D. Wright, C.-H. Lee and T. W. Shannon (1993) VIMS sea carousel: A field instrument for studying sediment transport. *Marine Geology*, **115**, 271–287.

Madsen O. S. and P. N. Wikramanayake (1991) *Simple model for turbulent wave–current bottom boundary layer flow*, DRP-91-1, Ralph M. Parsons Laboratory, Massachusetts Institute of Technology, Cambridge, MA, 150 pp.

Madsen O. S., L. D. Wright, J. D. Boon and T. A. Chisholm (1993) Wind stress, bed roughness, and sediment suspension on the inner shelf during an extreme storm event. *Continental Shelf Research*, **13**, 1303–1324.

Mason C., W. A. Birkemeier and P. A. Howd (1987) Overview of Duck 85 nearshore processes experiment. In: *Coastal sediments* '87, N. Kraus, editor, *ASCE*, pp. 818–833.

Miller M. C. and P. D. Komar (1980a) Oscillation sand ripples generated by laboratory apparatus. *Journal of Sedimentary Petrology*, **50**, 173–182.

Miller M. C. and P. D. Komar (1980b) A field investigation of the relationship between oscillation ripple spacing and the near-bottom water orbital motion. *Journal of Sedimentary Petrology*, **50**, 183–191.

Nielsen P. (1979) *Some basic concepts of wave sediment transport*, Series Paper No. 20, Institute of Hydrodynamics and Hydraulic Engineering, Technical University of Denmark.

Nielsen P. (1981) Dynamics and geometry of wave generated ripples. *Journal of Geophysical Research*, **86**, 6467–6472.

Nielsen P. (1983) Analytical determination of nearshore wave height variation due to refraction shoaling and friction. *Coastal Engineering*, **7**, 233–251.

Owen P. R. (1964) Saltation of uniform grains in air. *Journal of Fluid Mechanics*, **20**, 225–242.

Smith J. D. and S. R. McLean (1977) Spatially averaged flow over a wavy surface. *Journal of Geophysical Research*, **82**, 1735–1746.

Wiberg P. L. and C. K. Harris (1994) Ripple geometry in wave dominated environments. *Journal of Geophysical Research*, **99**(C1), 775–7879.

Wiberg P. L. and D. M. Rubin (1989) Bed roughness produced by saltating sediment. *Journal of Geophysical Research*, **94**, 5011–5016.

Wilson K. C. (1966) Bed-load transport at high shear stress. *Journal of the Hydraulics Division, ASCE*, **92**(HY6), 49–59.

Wilson K. C. (1988) *Friction behavior of sheet flow*, Progress Report No. 67, Institute of Hydrodynamics and Hydraulic Engineering, Technical University of Denmark.

Wilson K. C. (1989) Friction of wave-induced sheet flow. *Coastal Engineering*, **12**, 371–379.

Wright L. D. (1993) Micromorphodynamics of the inner continental shelf: A Middle Atlantic Bight case study. *Journal of Coastal Research*, (15), 93–124.

Wright L. D., J. D. Boon, M. O. Green and J. H. List (1986) Response of the mid shoreface of the southern Mid-Atlantic Bight to a "Northeaster". *Geo-Marine Letters*, **6**, 153–160.

Wright L. D., J. D. Boon, S. C. Kim and J. H. List (1991) Modes of cross-shore sediment transport on the shoreface of the Middle Atlantic Bight. *Marine Geology*, **96**, 19–51.

Wright L. D., J. D. Boon, J. P. Xu and S. C. Kim (1992) The bottom boundary layer of the bay stem plains environment of lower Chesapeake Bay. *Estuarine, Coastal and Shelf Science*, **35**, 17–36.

Wright L. D., J. P. Xu and O. S. Madsen (1994) Across-shelf benthic transports on the inner shelf of the Middle Atlantic Bight during the "Halloween storm" of 1991. *Marine Geology*, **118**, 61–77.